J. Electrochem. Sci. Eng. **16** (2026) 3001; https://doi.org/10.5599/jese.3001

Open Access : : ISSN 1847-9286
https://pub.iapchem.org/ojs/index.php/JESE

Original scientific paper

Determination of acetaminophen and theophylline in drug samples by electrochemical method using Fe/MCM-41 modified electrode

Huynh Thanh Danh[1,2], Nguyen Chi Bao[3], Pham Thi Huyen Thoa[4], Nguyen Quang Man[5], Pham Dinh Du[6] and Dinh Quang Khieu[1,✉]

[1]*University of Sciences, Hue University, Vietnam*
[2]*Giong Rieng High School, An Giang province, Vietnam*
[3]*Department of Science, Technology and International Relations, Hue University, Vietnam*
[4]*Department of Natural Sciences & Technology, Tay Nguyen University, Vietnam*
[5]*University of Medicine and Pharmacy, Hue University, Vietnam*
[6]*Thu Dau Mot University, Vietnam*

Corresponding Author: ✉dqkhieu@hueuni.edu.vn

Received: September 16, 2025; Accepted: January 28, 2026; Published: February 23, 2026

Abstract

In this study, we developed an electrochemical sensor based on an Fe/MCM-41 modified electrode for the simultaneous analysis of acetaminophen (AT) and theophylline (TP). The Fe/MCM-41 material was produced from diatomite silica and ferric chloride salts via a hydrothermal method. The synthesized material was characterized by XRD, SEM, TEM, EDX mapping, and nitrogen adsorption-desorption isotherms. Results showed that the Fe/MCM-41 maintained its mesoporous structure, high surface area, and uniform dispersion of Fe ions. Electrochemical tests revealed that the Fe/MCM-41 electrode exhibits superior electrocatalytic activity and higher current responses for both analytes than the bare electrode. The two oxidation peaks of AT and TP were distinctly separated, enabling simultaneous quantification of drugs with high selectivity. The peak current increased linearly with AT and TP concentrations from 0.50 to 14.15 µM, with detection limits of 0.430 and 0.350 µM, respectively. Notably, the sensor was successfully used to analyze pharmaceutical formulations containing one or both active substances, with satisfactory recoveries. The results confirm that the Fe/MCM-41 electrode is a promising sensing platform for the simultaneous analysis of AT and TP, opening new possibilities for pharmaceutical testing.

Keywords

Electrochemical sensor; modified glassy carbon electrode; mesoporous silica; doped iron; simultaneous drug analysis; real samples

Introduction

Acetaminophen (N-acetyl-para-aminophenol, $C_8H_9NO_2$, denoted as AT) is one of the most commonly used analgesics and antipyretics, thanks to its high therapeutic efficacy and relative safety at usual doses [1]. However, overdose of AT can cause serious toxicity to the liver and kidneys, so monitoring the concentration of this active ingredient in pharmaceutical preparations as well as in biological samples is of great clinical importance [2]. In parallel, theophylline (1,3-dimethylxanthine (or 3,7-dihydro-1,3-dimethyl-1H-purine-2,6-dione, $C_7H_8N_4O_2$, denoted as TP), a xanthine derivative [3], is still a widely prescribed bronchodilator in the treatment of asthma and chronic obstructive pulmonary disease (COPD) [4]. The difference of TP is its very narrow therapeutic range, and even small changes in plasma drug concentrations can lead to poor therapeutic efficacy or serious toxicity such as arrhythmias and convulsions [5]. Given the possibility of co-administration in the same patient, the need for simultaneous analysis of AT and TP has become increasingly important for both therapeutic monitoring and quality control of combination pharmaceutical preparations [5].

Many analytical techniques have been successfully applied for the simultaneous or individual quantification of these two active substances, such as high-performance liquid chromatography (HPLC) [5,6], high-performance liquid chromatography-ultraviolet (HPLC-UV) [7], magnetic-assisted ionic liquid-based microextraction method [8] for AT, HPLC [6], liquid chromatography-mass spectrometry [3] for TP, and the HPLC [5] for simultaneous AT and TP analysis. However, these methods often require complex sample handling, long analysis times and high equipment costs, which limit their application in routine monitoring or rapid on-site analysis. In contrast, electrochemical methods are recognized as robust approaches due to their high sensitivity, short analysis times, low cost and potential for integration into portable devices, allowing rapid and direct monitoring. The challenge is to ensure selectivity, as the oxidation potentials of AT and TP can overlap with conventional electrodes [9]. To overcome this limitation, chemically modified electrodes have been widely studied to enhance electrocatalytic activity, lower oxidation potentials, and improve analyte signal separation [10]. Among them, the mesoporous silica material MCM-41, with its large surface area, regular pore structure, and tunable pore size, is a promising platform for electrode modification. Doping multivalent metals [11], ferrites [12], and graphene oxide [13] into the MCM-41 framework can increase electron-transfer efficiency *via* a catalytic resonance effect, thereby improving the sensitivity and selectivity of the modified electrodes. Fe/MCM-41 is a material based on mesoporous silica with a large surface area, with an active catalytic centre that shows the ability to catalyse the photochemical degradation of Rhodamine B [14], the oxidative degradation of chitosan like heterogeneous Fenton catalyst [15], and the adsorption of the antibiotic oxytetracycline [16]. It becomes a promising candidate for the fabrication of electrochemical sensors. Hasanzadeh *et al.* [17] analysed amino acids using an MCM-41 (Fe_3O_4) modified electrode. Although there have been many reports on the use of modified electrodes for the individual analysis of AT or TP, studies on the simultaneous analysis of these two active substances on the same electrode surface are still limited [9]. In particular, the application of metal-doped mesoporous materials such as Fe/MCM-41 for electrochemical sensing has not been widely exploited, despite the high surface area, good dispersion of catalysts, and high chemical stability of this material. This research gap suggests great potential for developing a sensor system that is both highly sensitive and highly selective for simultaneous analysis. Therefore, the objective of this study was to fabricate and characterize a Fe/MCM-41-modified electrode and evaluate its applicability for the simultaneous analysis of acetaminophen and theophylline. This study not only provides scientific evidence for the superiority of Fe/MCM-41 in electrochemical sensors but also opens up new application prospects in drug quality monitoring.

Experimental

Materials

Diatomite was obtained from Phu Yen province, Vietnam. Raw diatomite was removed of organic impurities by washing and sedimentation with water several times, filtered, dried at 100 °C, and stored in sealed bags for further experiments.

N-cetyl-N,N,N-trimethylammonium bromide (> 96 %, n-$C_{16}H_{33}(CH_3)_3NBr$, CTAB), iron chloride hexahydrate (99 % $FeCl_3{\times}6H_2O$), acetaminophen ($C_8H_9NO_2$), and theophylline ($C_7H_8N_4O_2$) were purchased from Merck, Germany. Potassium chloride (99.5 % KCl), hydrochloric acid (37 % HCl), and sodium hydroxide (97 % NaOH) were obtained from Guangdong, China. The chemicals were of analytical grade and used without further purification.

Synthesis of MCM-41 with silica source from diatomite

The preparation of MCM-41 using diatomite as the silica source followed the method described by Yu *et al.* [18]. The procedure was carried out as follows: First, a mixture was prepared by adding 0.34 g of solid NaOH, 8.5 g of distilled water and 0.9 g of diatomite into a Teflon-lined steel reaction vessel, then heated at 150 °C for 4 hours; this was called mixture A. Separately, 1.09 g of CTAB was dissolved in 16.62 g of distilled water and stirred gently for 15 minutes to form mixture B. Mixtures A and B were then combined, and the pH of the resulting suspension was adjusted by gradually adding 16 to 22 mL of 0.2 M HCl to produce mixture C. The mixture C was transferred to a Teflon-lined steel reaction vessel and placed in a drying oven at a temperature ranging from 60 to 200 °C for a period of 15 to 72 hours. After hydrothermal treatment, the solid product was filtered, washed with distilled water until neutral, dried, and then calcined at 550 °C for 6 hours. In this way, the mesoporous material MCM-41 was obtained.

Preparation of Fe/MCM-41

The modification of MCM-41 with iron was carried out as follows.: A solution containing 5.0 mmol of $FeCl_3{\times}6H_2O$ (1.3516 g) in 30 mL of distilled water was slowly dropped into 150 mL of boiling distilled water to form a $Fe(OH)_3$ colloidal system. Then, 1.0 g of the previously prepared MCM-41 was placed into a 200 mL steel-coated Teflon vessel, and the entire $Fe(OH)_3$ colloidal system was transferred into the vessel. The Teflon vessel containing the reaction mixture was placed in a drying oven at 100 °C for 6 hours. After cooling to room temperature, the solid product was filtered, washed several times with distilled water, and dried at 100 °C. In this way, the Fe/MCM-41 material was obtained.

Apparatus

The X-ray diffraction (XRD) was conducted on a D8 Advance Bruker (Germany). Transmission electron microscopy (TEM) was performed using a JEOL JEM-2010F transmission electron microscope. The nitrogen adsorption-desorption isotherms were measured on a Tristar-3030 system (Micromeritics, USA). Elemental mapping by energy-dispersive X-ray spectroscopy was carried out using a Hitachi S-4800 FESEM (Japan) scanning electron microscope equipped with an energy-dispersive X-ray (EDX) system. Electrochemical measurements were taken with a CPA-HH5 electrochemical workstation (Vietnam) in a standard three-electrode setup. A glassy carbon electrode (GCE, 2.8 mm diameter, modified with the synthesized material) served as the working electrode; a platinum wire functioned as the counter electrode; and an Ag/AgCl (3 M KCl) electrode was used as the reference electrode. All experiments were performed in 0.1 M Britton-Robinson (BR) buffer solution at room temperature.

Preparation of working electrode

The GCE was polished using 0.05 µm aluminium oxide powder. Next, the GCE was immersed in 1 M HNO_3 solution, absolute ethanol, and distilled water to remove any remaining aluminium oxide powder. A 1 mg mL^{-1} modifier suspension was prepared by dispersing 5 mg of modifier (Fe/MCM-41 or MCM-41) in 5 mL of distilled water, followed by sonication for 5 hours. The electrode was modified by dropping 5 µL of the modifier suspension onto its surface and allowing it to dry naturally at room temperature.

Electrochemical measurements

The electrochemical properties of the working electrode modified with different materials were investigated by cyclic voltammetry (CV) curves recorded in 0.02 M Britton-Robinson (BR) buffer, pH 5, at a scan rate of 0.2 V s^{-1} in the potential range from 0.0 to 1.7 V until repeatable peak-potential curves were obtained. The differential pulse voltammetry (DPV) technique, under optimal parameter conditions, was investigated for AT and TP analysis on modified electrodes.

Pharmaceutical sample processing

Ten pharmaceutical units (powder or tablets) were carefully weighed, and the average mass of the ten units was determined. The units were finely ground in a mortar, and an appropriate amount of the resulting powder was measured into a 100 mL volumetric flask. About 50 mL of water was added, and the mixture was dissolved and sonicated for approximately 30 minutes. After cooling, the solution was adjusted to volume with water, shaken thoroughly, and filtered through filter paper to produce solution 1. A portion of the filtrate was then diluted with water to a suitable concentration to produce solution 2. An exact volume of solution 2 was then pipetted into an electrochemical cell and diluted to 10 mL with 0.02 M BR buffer solution. DPV analysis was then carried out using the optimized parameters to determine the AT/TP content in each sample.

Results and discussion

Materials characterization

Figure 1 presents some physicochemical characteristics of the synthesized material. The small-angle X-ray diffraction (XRD) pattern of MCM-41 shows a highly ordered hexagonal structure corresponding to the diffractions 2θ = 2.4° (100), 4.1° (110) and 4.8° (200) [18] (Figure 1A).

When Fe is doped, the (100) diffraction peak still exists, but the intensity is reduced, while the 2D structure of MCM-41 is significantly changed, corresponding to the diffractions (110) and (200) not observed. This result also shows that when Fe is doped, the 2D structure of MCM-41 changes but still retains part of the mesoporous structure. The large-angle XRD pattern in Figure 1B does not show any diffraction except for the broad diffraction at 28° characteristic of amorphous silica. This result suggests that the modified oxides mainly exist in the amorphous form. The FT-IR spectra of MCM-41 and Fe/MCM41 are shown in Figure 1C. In all samples, the characteristic bands of the MCM-41 framework are clearly visible [19]. The broad bands around 3500 cm^{-1} can be attributed to the surface silanols and adsorbed water molecules, while the bending vibrations of the adsorbed water molecules cause the absorption bands at 1623 to 1640 cm^{-1} [20]. The slight shift of the 1109 cm^{-1} band of Si-O-Si to the 1081 cm^{-1} band of Si-O-Fe vibrations allows us to conclude that heteroatoms have been introduced into the MCM-41 framework and the formation of Si-O-Fe bonds [20,21]. This shift is due to the increase in the average Si-O distance caused by the substitution of small silicon (radius 40 pm) by larger Fe^{3+} (radius 63 pm) [21]. The observed changes,

which depend on both the change in ionic radius and the degree of substitution, are relatively small, so only low degrees of substitution are indicated.

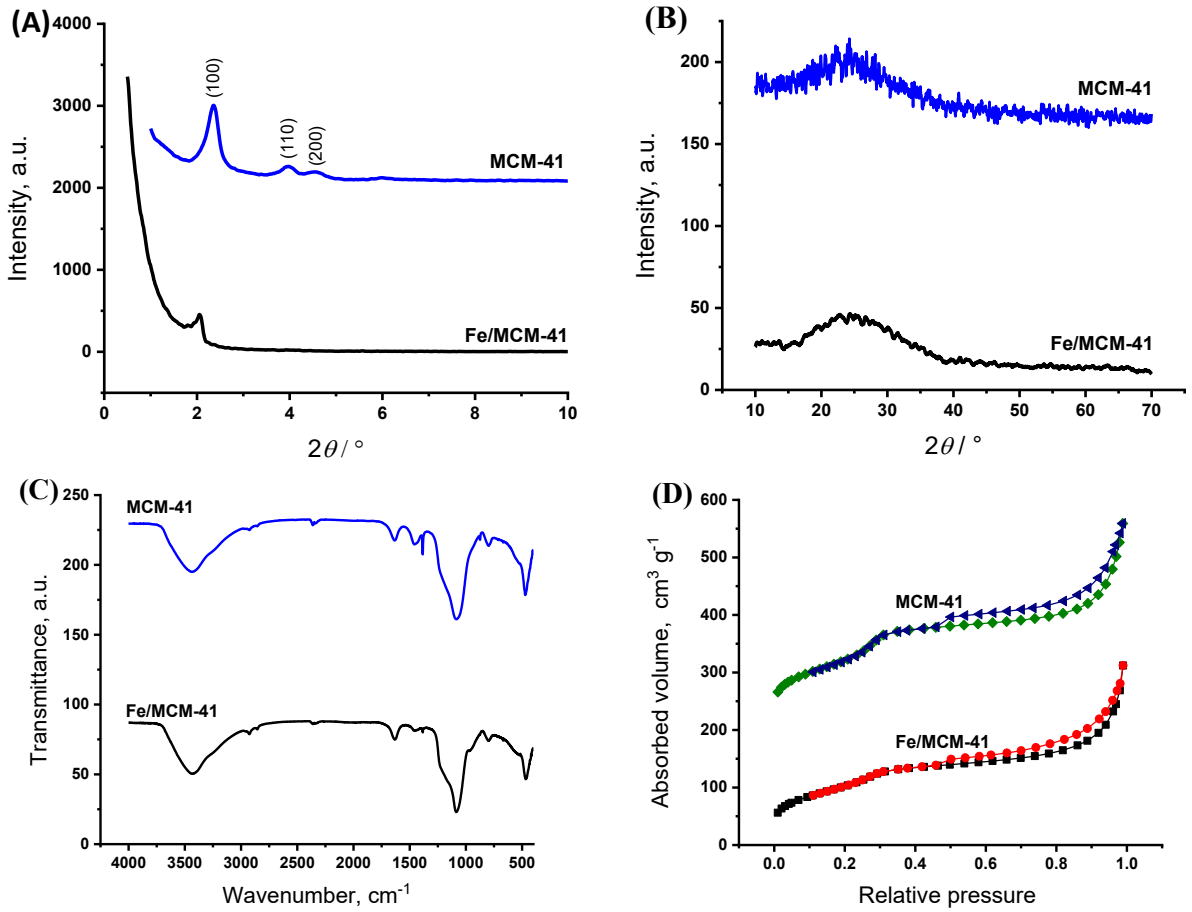

Figure 1. *(A) Small-angle XRD patterns, (B) wide-angle XRD patterns, (C) FT-IR spectra and (D) N_2 adsorption - desorption isotherms of MCM-41 and Fe/MCM-41*

The N_2 adsorption-desorption isotherms of MCM-41 and Fe/MCM-41 are presented in Figure 1d. All samples exhibit type IV isotherms according to the IUPAC classification. Three distinct stages can be identified: an initial slow increase in nitrogen uptake at low relative pressure, corresponding to monolayer-multilayer adsorption on the pore walls; a sharp step at intermediate relative pressure, indicating capillary condensation in the ordered mesopores; and finally, a hysteresis loop at high relative pressure, which is associated with interparticle mesopores. The porous structure of MCM-41 was largely preserved after Fe incorporation.

The textural properties are summarized in Table 1. The specific surface area of MCM-41 decreased from 443.5 to 373.3 $m^2\ g^{-1}$ upon Fe doping. Moreover, a significant change in the contribution of the microporous area was observed, increasing from 14.6 % to 33.9 %. These results suggest that the introduction of Fe affects both the surface area and pore volume of MCM-41. The lower surface area of Fe/MCM-41 compared with pristine MCM-41 may be related to the higher incorporation of Fe species into the framework.

Table 1. *Textural properties of the synthesized materials*

Sample	BET surface area, $m^2\ g^{-1}$	Micropore area, $m^2\ g^{-1}$	Mesopore area, $m^2\ g^{-1}$	Micropore volume, $cm^3\ g^{-1}$
MCM-41	443.5	64.7	378.8	0.1872
Fe/MCM-41	373.3	125.2	248.1	0.1386

Figure 2 shows the morphologies of MCM-41 and Fe/MCM-41. The (100) and (110) diffraction planes were clearly observed, confirming the materials' ordered mesoporous structure. For Fe/MCM-41, Fe species were dispersed as spherical nanoparticles with diameters of only a few nanometres on the MCM-41 surface, while the (110) plane was still detectable. These observations are consistent with the XRD and BET results, indicating that the mesoporous ordering of MCM-41 decreased upon Fe incorporation.

The elemental composition of the synthesized samples was analysed by EDX (Figure 3). The EDX spectrum of pristine MCM-41 (Figure 3a) shows the presence of Si as the main framework element, along with minor impurities such as Fe, Ti, and Al originating from the natural diatomite precursor. After Fe incorporation, the Fe content increased markedly in Fe/MCM-41 (Figure 3b). Furthermore, the EDX mapping images of Fe/MCM-41 (Figures 4A to 4G) confirmed the homogeneous distribution of Fe within the MCM-41 framework.

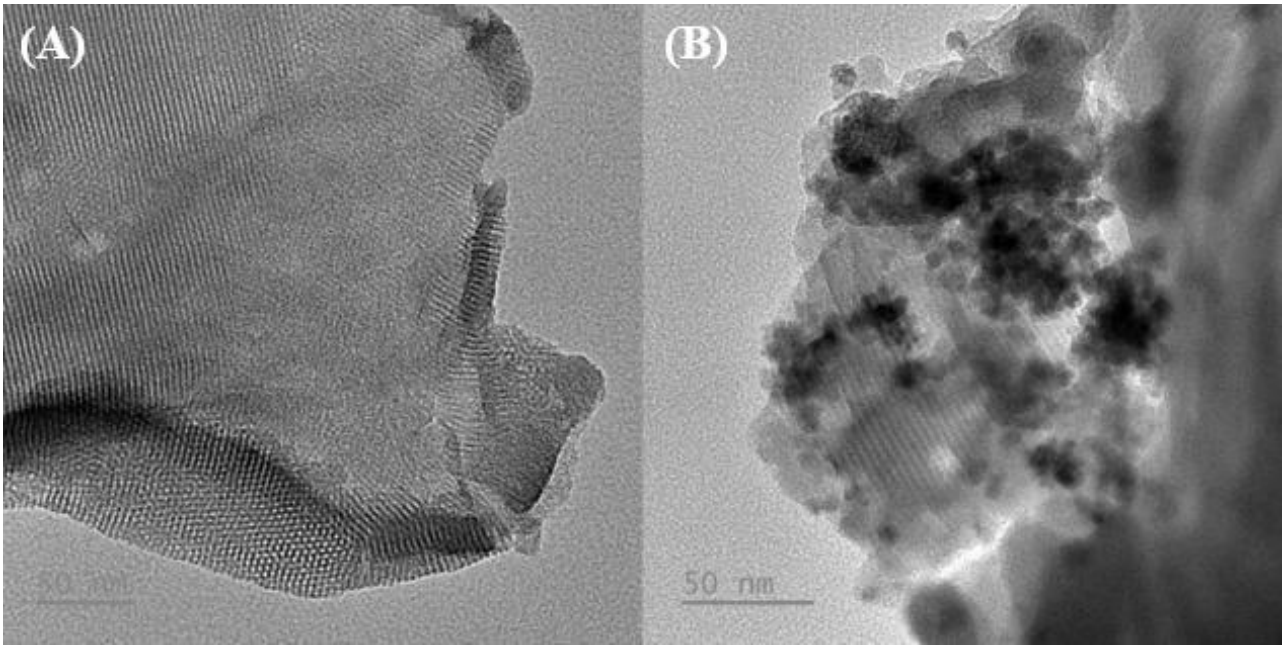

Figure 2. *TEM images: (A) MCM-41 and (B) Fe/MCM-41*

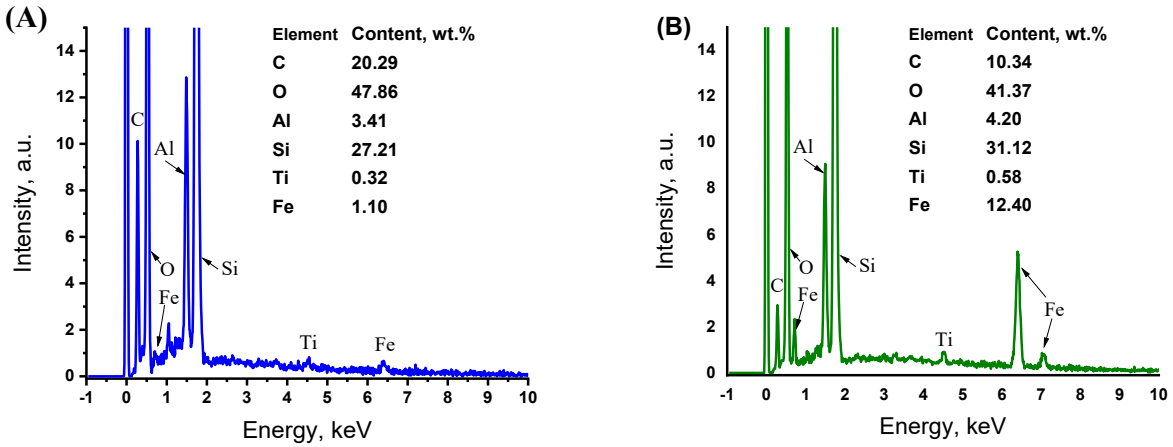

Figure 3. *EDX spectra of (A) MCM-41 and (B) Fe/MCM-41*

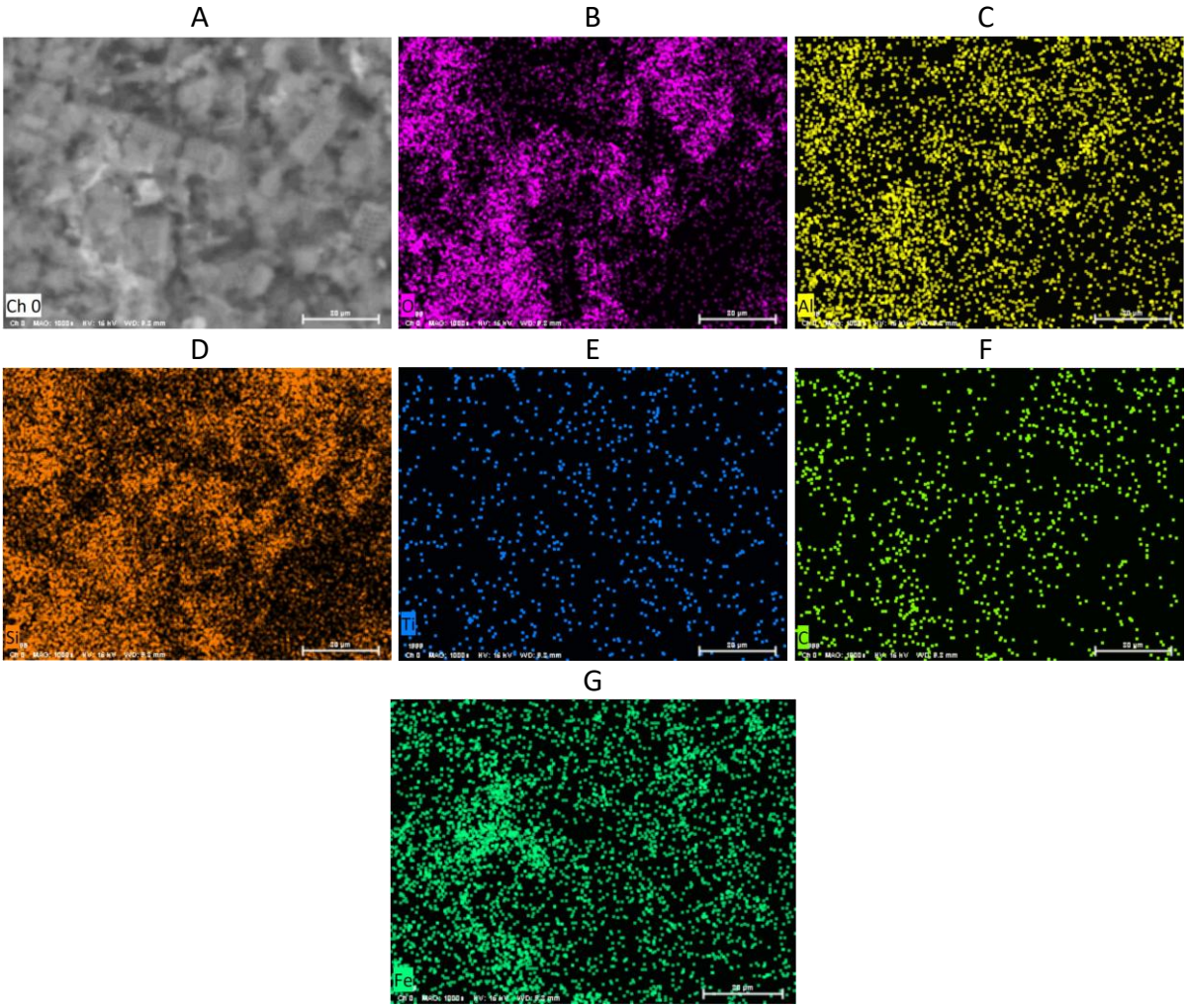

Figure 4. *EDX mapping images of elemental distribution of Fe/MCM-41: A - complete electron image; B - oxygen; C - aluminium; D - silicon; E - titanium; F - carbon and G - iron distribution*

Electrochemical behaviour of AT and TP on different electrodes

Figure 5 shows the CV curves of AT and TP on different electrodes in the BR buffer (pH 5) solution. The bare GCE showed a weak AT oxidation signal, while the TP signal was not observed.

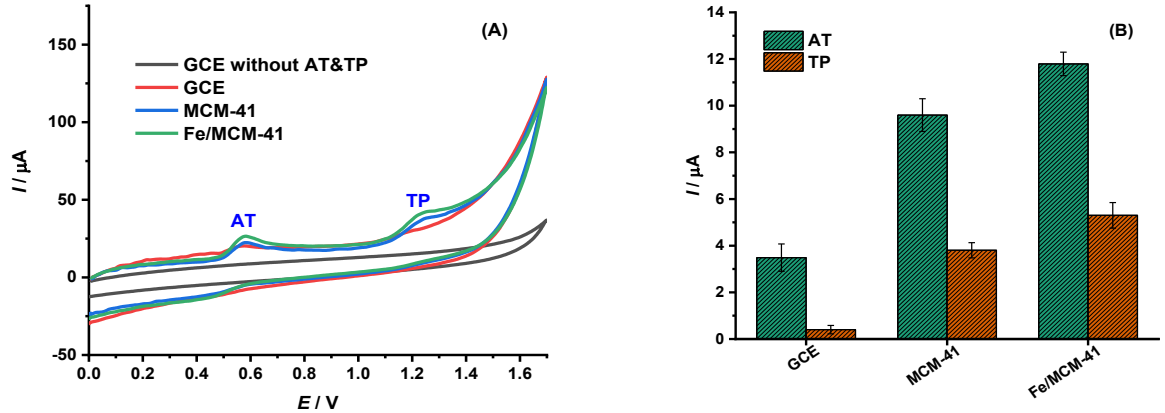

Figure 5. *(A) CVs (cycle voltammograms) of different electrodes with C_{AT} = C_{TP} = 12.5 µM in 0.02 M BR buffer (pH 5), scanning rate v = 0.2 V s^{-1}; (B) oxidation peak intensities of AT and TP at different electrodes (3 replicate measurements)*

When modified with MCM-41, the AT oxidation signal at about 0.6 V and TP at 1.2 V increased significantly. In particular, when MCM-41 was doped with Fe, the signal increased 1.3 times

compared to MCM-41. The Fe/MCM-41/GCE electrode showed the highest and most stable signal intensity.

Effect of pH

Figure 6 shows the effect of pH on the CV signals. There is a clear shift of the oxidation potentials of AT and TP towards the less positive values as pH increases (Figure 6A), indicating that the oxidation process on the modified electrode involves proton exchange. The relationship between peak potential and pH can be expressed through the Nernst equation (Figure 6B) and is presented in Equations (1) and (2).

$$E_{AT} = (0.8482 \pm 0.0082) + (-0.0500 \pm 0.0013)\ \text{pH};\ R^2 = 0.995 \quad (1)$$

$$E_{TP} = (1.4660 \pm 0.0151) + (-0.0520 \pm 0.0023)\ \text{pH};\ R^2 = 0.986 \quad (2)$$

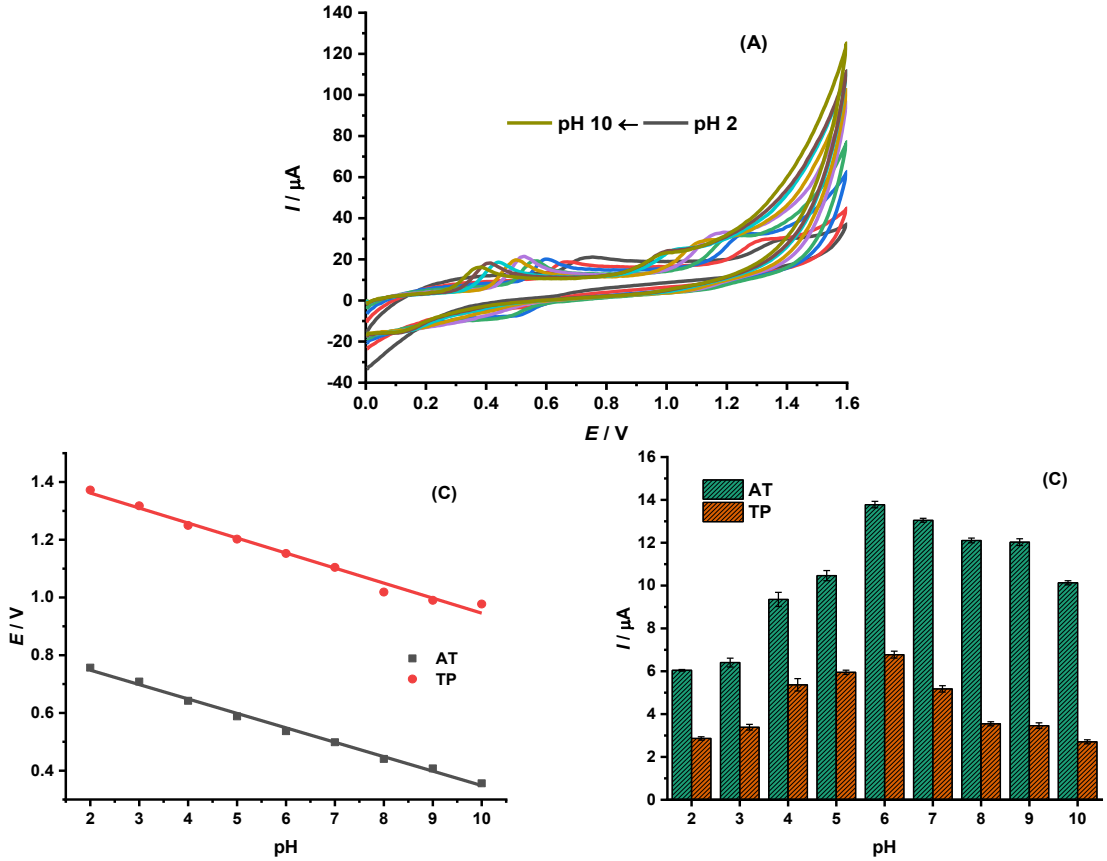

Figure 6. *(A) CV curves of Fe/MCM-41/GCE in 0.02 M BR buffer (pH 2 to 10) with $C_{AT} = C_{TP} = 12.5$ µM, potential scanning rate $\nu = 0.2$ V s^{-1}; (B) linear regression curves between oxidation potentials E_{AT} and E_{TP} and pH values; (C) oxidation peak current intensities of AT and TP at different pH values*

There is a high linear correlation of AT and TP oxidation potentials with pH (R^2 = 0.986-0.995). The slope of the straight line with slope coefficient -0.0500 V pH^{-1} for AT and -0.0520 V pH^{-1} for TP is very close to the theoretical value -0.059 V pH^{-1} corresponding to an equal number of protons and electrons exchanged. Therefore, it can be concluded that the oxidation process of AT and TP has the same number of electrons and protons exchanged. Figure 5C shows that the oxidation current intensity of AT and TP varies with pH. The current intensity increases gradually from 2 to 6, then decreases as the pH continues to rise. Therefore, a buffer solution at pH 6 is used for subsequent studies. Based on previous studies [22,23], the oxidation reaction of AT and TP at the electrode proceeds via a mechanism in which the number of transferred electrons equals the number of exchanged protons, as illustrated in Scheme 1.

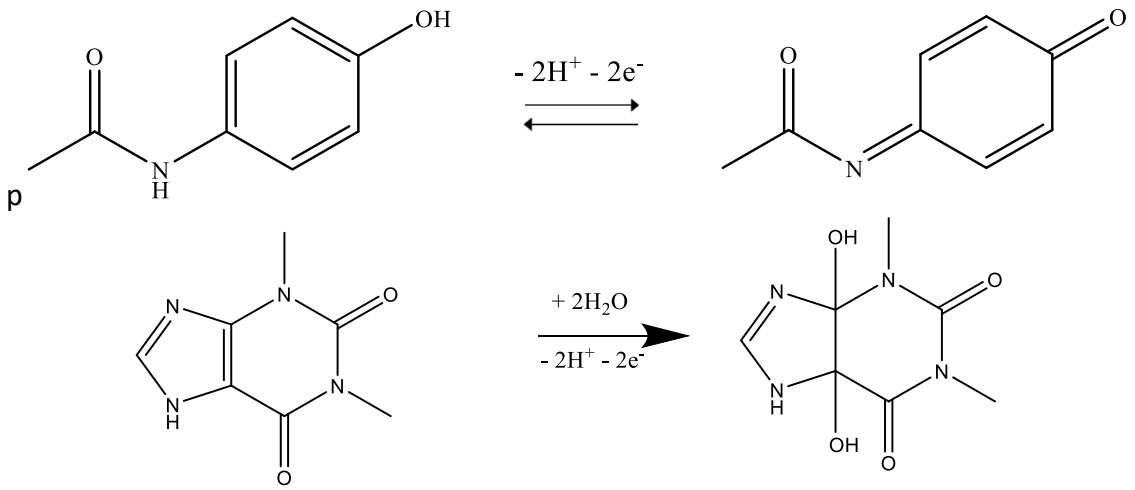

Scheme 1. *Proposed illustrative oxidation mechanism of AT and TP at the modified electrode in an aqueous medium*

Investigation of optimal parameters of differential pulse voltammetry

The working parameters, including accumulation potential, accumulation time, pulse amplitude and voltage step of the DPV method, were also investigated and presented in Figures S1 to S4 of the Supplementary material. Based on the peak current intensity and stability, we found that the optimal accumulation potential, accumulation time, pulse amplitude and potential step for the highest and most stable current intensity were 0 V, 5 s, 0.11 V and 0.007 V, respectively.

Linear range and mutual interference

In this experiment, we gradually increased the AT and TP concentrations from 0.50 to 14.15 µM. Figure 7a shows the DPV curves recorded for the simultaneous determination of AT and TP. The concentrations of both analytes were increased simultaneously, resulting in a proportional increase in the corresponding oxidation peak currents. The linear relationships between peak currents and analyte concentrations are shown in Figure 7b. The linear relationship with a high coefficient (R^2 = 0.999) is shown in Equations (5) and (6). The limit of detection (LOD) determined by the 3σ rule was 0.43 µM for AT and 0.35 µM for TP, respectively.

$$I_{AT} = (3.821 \pm 0.095) + (1.167 \pm 0.012)\, C_{AT};\ R^2 = 0.999 \quad (5)$$

$$I_{TP} = (0.084 \pm 0.037) + (0.562 \pm 0.005)\, C_{TP};\ R^2 = 0.999 \quad (6)$$

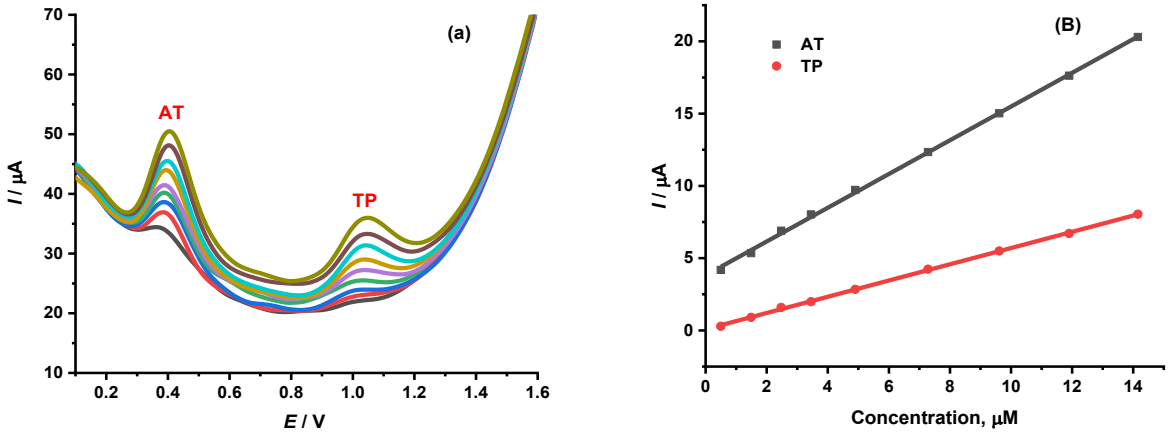

Figure 7. *(A) DPV curves of Fe/MCM-41/GCE in 0.02 M BR buffer (pH 6) with C_{AT} = C_{TP} = 0.50 to 14.15 µM; (B) linearity between peak current and AT or TP concentration*

To evaluate possible cross-interference between the two analytes, the concentration of TP was fixed at 14.15 µM while the concentration of AT was varied from 0.50 to 14.15 µM, and *vice versa*, with AT fixed at 14.15 µM and TP varied within the same range (Figure 8). It was found that DPV responses were obtained by increasing AT concentration while keeping TP constant. The oxidation peak current of AT increased gradually with concentration, whereas the peak response of TP remained nearly unchanged, indicating negligible interference from TP. Conversely, the DPV curves were recorded by varying the TP concentration while keeping the AT concentration fixed. A proportional increase in the TP oxidation peak current was observed, while the AT peak current showed negligible variation. The obtained linear regression are defined by Equations (7) and (8):

$$I_{AT} = (1.849 \pm 0.077) + (1.277 \pm 0.010)\, C_{AT};\ R^2 = 0.999;\ \mathrm{LOD}_{AT} = 0.320\ \mu\mathrm{M} \quad (7)$$

$$I_{TP} = (0.042 \pm 0.031) + (0.565 \pm 0.004)\, C_{TP};\ R^2 = 0.999;\ \mathrm{LOD}_{TP} = 0.290\ \mu\mathrm{M} \quad (8)$$

The LODs (0.32 µM for AT and 0.29 µM for TP) are essentially comparable to those obtained in the simultaneous determination. These results demonstrate that cross-interference between AT and TP is negligible, confirming that the Fe/MCM-41/GCE electrode enables simultaneous analysis of AT and TP with high selectivity and accuracy.

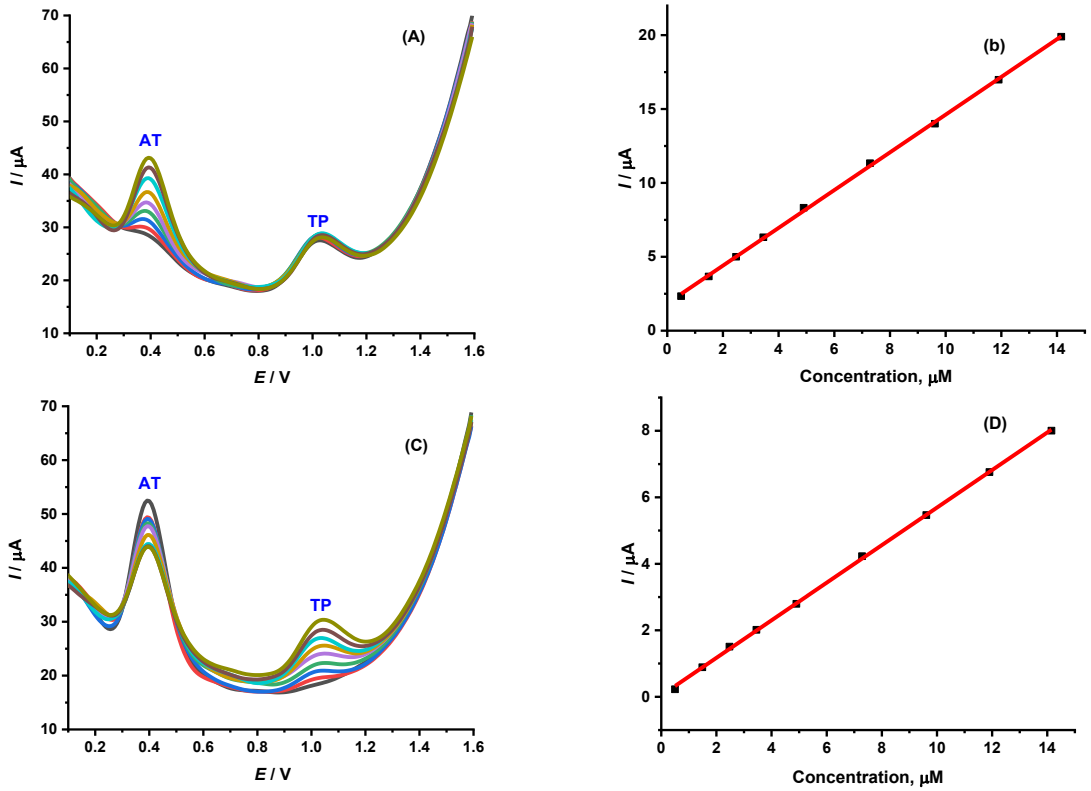

Figure 8. *(A) DPV curves of Fe/MCM-41/GCE in 0.02 M BR buffer (pH 6) with* C_{AT} *= 0.50 to 14.15 µM,* C_{TP} *= 14.15 µM; (B) linear curve between peak current and AT concentration; (C) DPVs with* C_{AT} *= 14.15 µM,* C_{TP} *= 0.50 to 14.15 µM; (D) linear curve between peak current and TP concentration*

Table 2 compares the LODs of AT and TP on Fe/MCM-41/GCE with those of other modified electrodes reported in the literature. The results show that the Fe/MCM-41/GCE developed in this work has LOD values of 0.430 µM (AT) and 0.350 µM (TP), which are competitive with those of many other electrodes. Some systems provide superior sensitivity, *e.g.* $Na_2Fe_4O_7$-NPs/GCE (LOD = 0.003 µM for AT) and SnS_2/GCE (LOD = 0.004 µM for TP). The main advantage of Fe/MCM-41/GCE is its ability to detect both AT and TP within the same linear range, whereas most other electrodes are designed for a single analyte.

Table 2. *Comparison of the detection performance for AT and TP at Fe/MCM-41/GCE with some other modified electrodes*

Electrode	Linear range, µM		LOD, µM		
	AT	TP	AT	TP	Ref.
Fe/MCM-41/GCE	0.50 to 14.15	0.50 to 14.15	0.430	0.350	This work
$Ti_3C_2T_x$ MXene/MWCNT/GCE	1.00 to 90.10	2.00 to 90.90	0.230	0.430	[9]
$CoFe_2O_4$/MCM-41/CPE	3.00 to 200.00	-	1.050	-	[12]
Polyurethane screen-printed composite electrode	1.00 to 40.00	-	1.200	-	[24]
$MnFe_2O_4$@CNT-N	1.0 to 1000	-	0.830	-	[25]
$Ni_{0.5}Mn_{0.5}Co_2O_4$	10 to 5000	-	2.000	-	[26]
β-cyclodextrin/GCE	0.10 to 80	-	0.097	-	[27]
$Na_2Fe_4O_7$-NPs/GCE	0.01 to 450	-	0.003	-	[28]
Poly(L-phenylalanine)-reduced graphene oxide/GCE	-	1.00 to 260	-	0.350	[29]
ZnONF/GO/BDDNPs/SPE	-	50 to 120	-	0.170	[30]
g-C_3N_4/GCE	-	5.2 to 118.0	-	0.043	[31]
SnS_2 nanoflake/GCE	-	0.01 to 0.25	-	0.004	[32]
CDs/GCE	-	10 to 5000	-	1.000	[33]

GCE: glassy carbon electrode; CPE: carbon paste electrode, MWCNT: multiwall carbon nanotubes; CNT-N: N-doped carbon nanotubes; ZnONF/GO/BDDNPs: ZnO nanoflowers/graphene oxide/boron-doped diamond nanoparticles; SPE: screen printed electrode; g-C_3N_4: graphitic carbon nitride; CDs: carbon dots

Repeatability, reproducibility and durability

The repeatability of the proposed DPV method was studied by measuring the DPV of AT and TP solutions at three different concentrations (2.48, 7.28 and 11.9 µM). At each concentration, the measurement was continuously repeated 10 times. Repeatability was assessed by comparing the relative standard deviation (RSD) of replicate measurements with ½ of the Horwitz RSD. The results are presented in Figure 9, while the average values of the peak current and the corresponding RSD are as follows:

$C_{AT} = C_{TP}$ = 2.48 µM (Figure 9A)

I_{AT} = 8.22 ± 0.39 µA; RSD = 4.73 % < ½ Horwitz RSD (9.28 %)

I_{TP} = 1.54 ± 0.06 µA; RSD = 4.13 % < ½ Horwitz RSD (9.03

$C_{AT} = C_{TP}$ = 7.28 µM (Figure 9B)

I_{AT} = 13.01 ± 0.41 µA; RSD = 3.17 % < ½ Horwitz RSD (7.89 %)

I_{TP} = 4.11 ± 0.16 µA; RSD = 3.78 % < ½ Horwitz RSD (7.68 %)

$C_{AT} = C_{TP}$ = 11.90 µM (Figure 9C)

I_{AT} = 16.04 ± 0.41 µA; RSD = 2.55 % < ½ Horwitz RSD (7.32 %)

I_{TP} = 6.27 ± 0.15 µA; RSD = 2.31 % < ½ Horwitz RSD (7.13 %)

It can be seen that the RSD values at different concentrations are all less than ½ of the corresponding Horwitz RSD values (Horwitz RSD = $2^{(1 - 0.5\log C)}$). This result demonstrates that the proposed method is highly repeatable.

To investigate the reproducibility of the method, the DPV of AT and TP were recorded on 7 electrodes modified in the same process (Figure 10A). The results showed that the current intensity values at the 7 electrodes varied as follows: I_{AT} = 12.93 ± 0.44 µA; RSD = 3.38 % and I_{TP} = 4.02 ± 0.12 µA; RSD = 3.01 %. In which the RSD was less than 5 %, indicating good reproducibility. The electrode stability was evaluated by measuring DPV signals for AT and TP on the same electrode over seven consecutive days. After each day, the electrode was kept in a pH 6 buffer at 4 °C in the refrigerator (Figure 10B). The peak current intensity after seven measurements on the same modified electrode varied as follows: I_{AT} = 12.76 ± 0.59 µA, RSD = 4.59 % and I_{TP} = 4.06 ± 0.11 µA, RSD = 2.59 %. The RSD is less than 5 %, indicating that the prepared electrode is relatively stable.

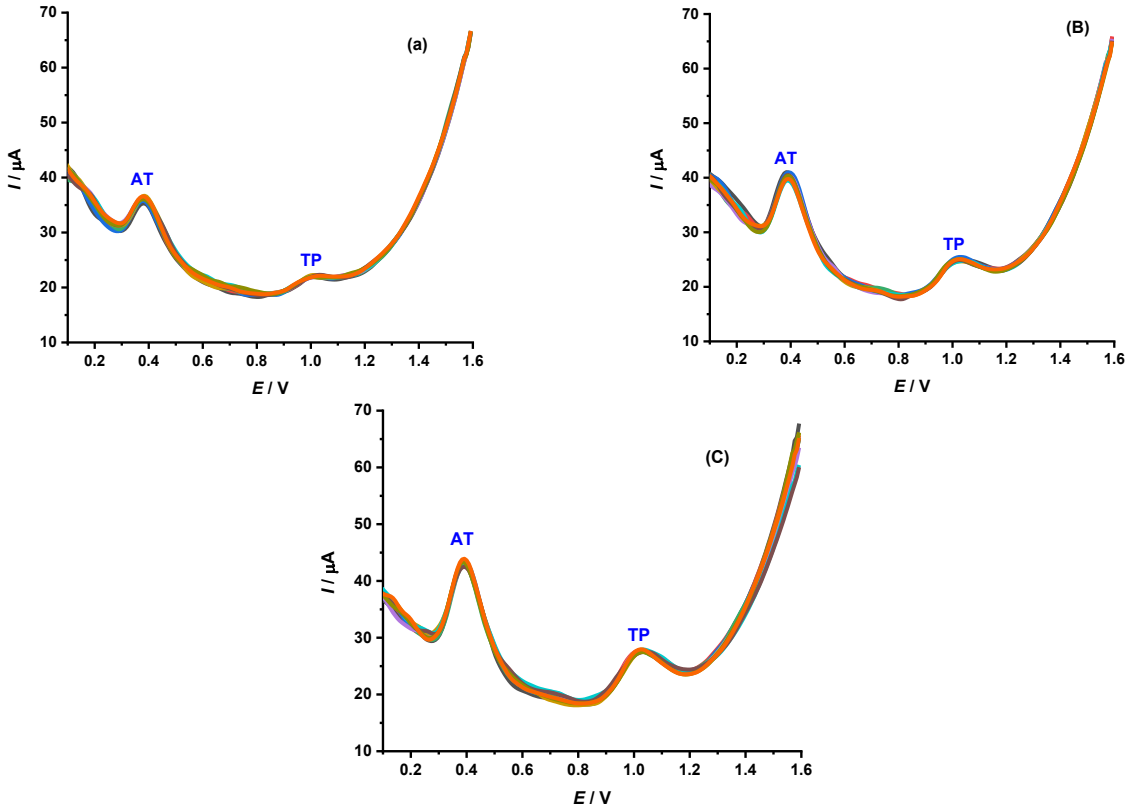

***Figure 9**. DPV curves of Fe/MCM-41/GCE in 0.02 M BR buffer (pH 6) with: (a) C_{AT} = C_{TP} = 2.48 µM; (B) C_{AT} = C_{TP} = 7.28 µM; and (C) C_{AT} = C_{TP} = 11.90 µM*

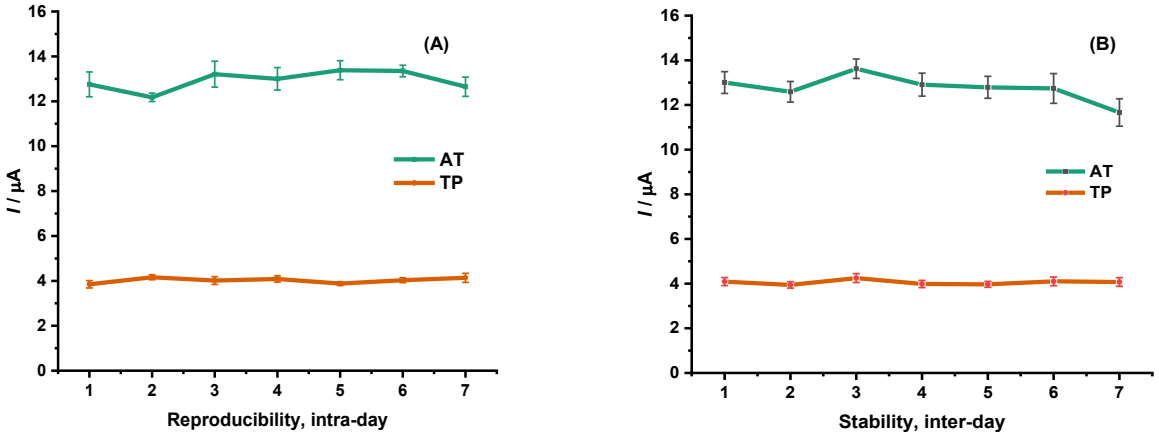

***Figure 10.** DPV peak currents of AT and TP (C_{AT} = C_{TP} = 7.28 µM) at Fe/MCM-41/GCE in 0.02 M BR buffer (pH 6) obtained on: (A) seven different electrodes prepared by the same procedure; (B) the same electrode after successive measurements while being stored in buffer solution at 4 °C*

Interference investigation

The accuracy of the method depends largely on the interferences present in the drug, some substances can coexist in drugs containing AT and TP such as KNO_3 (C1), $Al_2(SO_4)_3{\cdot}14H_2O$ (C2), NaCl (C3), $CaCl_2$ (C4), Na_2CO_3 (C5), D-glucose (C6), D-sucrose (C7), L-cysteine (C8), sodium benzoate (C9), glutamic acid (C10), ascorbic acid (C11) and caffeine (C12). A substance was regarded as non-influential when the absolute relative error, calculated as the percentage change in the response signal in the presence of a coexisting species, did not exceed 5 %.

Figure 11A shows that inorganic substances have little effect on the peak current (the x-axis represents the ratio of the molar concentration of the interfering substance to the AT or TP concentration), KNO_3, $CaCl_2$, Na_2CO_3, at concentrations 100 times higher still have no effect, $Al_2(SO_4)_3$ and NaCl when the concentration is 80 times higher. The studied organic substances also have little effect (Figure 11B). L-cysteine and sodium benzoate, at 100 times higher concentrations, also have no effect; the remaining substances, when the concentration exceeds 80 times, have an effect. This result proves that the proposed method has a high selectivity.

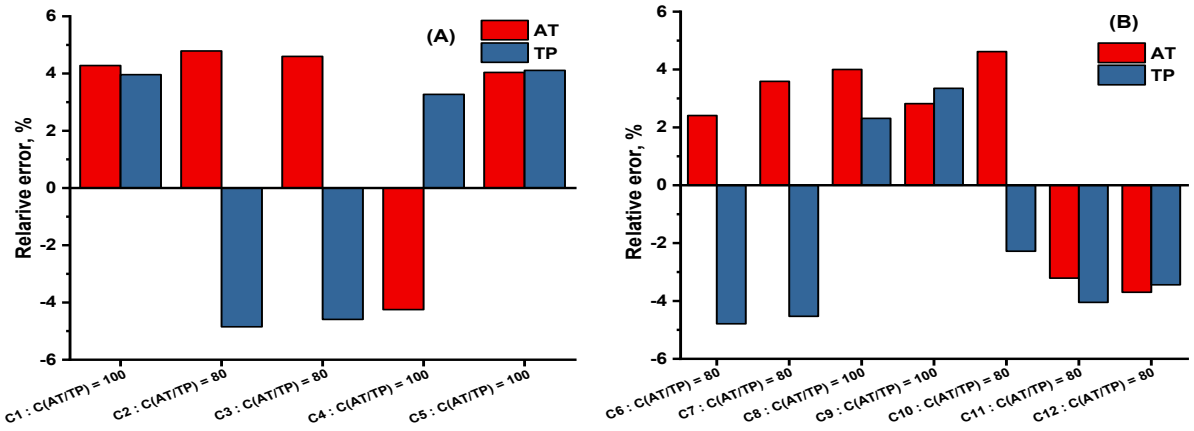

Figure 11. *Effects of some (A) inorganic and (B) organic interferents on peak current intensity values (relative error) of AT and TP at Fe/MCM-41/GCE in 0.02 M BR buffer (pH 6)*

Analysis of real samples

Five pharmaceutical samples containing AT or TP were analyzed using the proposed method. Known amounts of the corresponding standards were added to the samples, and the contents of AT and TP were determined in both real and spiked samples. The recovery values (Rev, %) were calculated and are summarized in Table 3. The results showed that the proposed method gave results that were not much different from the value stated on the label and the Rev varied between 94.09 and 103.91 %, which is acceptable. This result also confirmed the accuracy of the method.

Table 3. *Analysis of AT and TP in 05 pharmaceutical samples and three human urine samples*

Samples	Analyte	Content ± SD*, µM	Amount, µg		Rev, %
			Spiked	Found ± SD	
Hapacol 80 (label claim: 80 mg AT/unit) (Oral powders)	AT	82.12 ± 1.04	3.02	3.14 ± 0.08	103.91
	TP	-	3.60	3.39 ± 0.06	94.09
Hapacol 150 (label claim: 150 mg AT/unit) (Oral powders)	AT	146.82 ± 2.44	3.02	2.97 ± 0.09	98.17
	TP	-	3.60	3.46 ± 0.08	96.01
Hapacol 250 (label claim: 250 mg AT/unit) (Oral powders)	AT	244.79 ± 2.15	3.02	2.88 ± 0.05	95.16
	TP	-	3.60	3.71 ± 0.02	102.97
Theophylline extended-Release tablets (label claim: 100 mg TP/unit) (Oral powders)	AT	-	3.02	3.10 ± 0.04	102.55
	TP	97.52 ± 1.21	3.60	3.48 ± 0.03	96.50
Theolin tablets (label claim: 200 mg TP/unit) (Oral powders)	AT	-	3.02	2.91 ± 0.05	96.11
	TP	192.71 ± 3.76	3.60	3.50 ± 0.16	97.17
Human urine 1	AT	-	9.07	9.40 ± 0.16	103.66
	TP	-	5.40	5.28 ± 0.06	97.61
Human urine 2	AT	-	9.07	9.36 ± 0.17	103.15
	TP	-	5.40	5.48 ± 0.05	101.41
Human urine 3	AT	-	9.07	9.28 ± 0.13	102.34
	TP	-	5.40	5.12 ± 0.11	94.81

*Standard deviation

In addition, we evaluated the sensor's applicability in biological matrices. Three human urine samples were spiked with the same known concentrations of AT and TP, and the recovery values were determined. The obtained recovery values (94.81 to 103.63 %) demonstrate good accuracy in complex biological matrices. This additional evaluation further supports the practical applicability of the proposed method for real sample analysis.

Conclusions

The MCM-41 and Fe/MCM-41 materials were successfully synthesized with a silicon source from diatomite. The obtained materials have a high surface area, and Fe elements are evenly dispersed within the MCM-41 framework. Fe/MCM-41 can increase the electrochemical signals of AT and TP. This electrode has a low LOD (0.43 µM for AT and 0.35 µM for TP), a linear range for both AT and TP is from 0.50 to 14.15 µM and has high selectivity and stability. The Fe/MCM-41 material, with a high surface area and abundant electrocatalytic sites, is a promising modifier for developing new electrode platforms.

Supplementary material

Additional data are available at https://pub.iapchem.org/ojs/index.php/JESE/article/view/3001, or from the corresponding author on request.

Funding *This work is funded by Hue University under the Core Research Program No NCTB.DHH.2025.05.*

Conflict of interest: *The authors declare no conflict of interest.*

Author contributions: *Study conception and design: H.T.D, N.C.P.; data collection: P.T.H.T, N.Q.M; analysis and interpretation of results: P.D.D. The first and final draft of the manuscript was written by H.T.D and D.Q.K. and all authors commented on previous versions of the manuscript. All authors read and approved the final manuscript.*

References

[1] E. N. Mezaal, K. A. Sadiq, M. M. Jabbar, T. H. Al-Noor, E. A. Azooz, E. A. J. Al-Mulla, Green methods for determination of paracetamol in drug samples: A comparative study, *Green Analytical Chemistry* **10** (2024) 100123. https://doi.org/10.1016/j.greeac.2024.100123

[2] C. Pasha, Determination of paracetamol in pharmaceutical samples by spectrophotometric method, *Eclética Química* **45** (2020) 37-46. https://doi.org/10.26850/1678-4618eqj.v45.3.2020.p37-46

[3] H. Kanazawa, R. Atsumi, Y. Matsushima, J. Kizu, Determination of theophylline and its metabolites in biological samples by liquid chromatography-mass spectrometry, *Journal of Chromatography A* **870** (2000) 87-96. https://doi.org/10.1016/s0021-9673(99)00891-2

[4] P .J. Barnes, Theophylline, *American Journal of Respiratory and Critical Care Medicine* **188** (2013) 901-906. https://doi.org/10.1164/rccm.201302-0388PP

[5] T. A. P. Fernandes, J. P. Aguiar, A. I. Fernandes, J. F. Pinto, Quantification of theophylline or paracetamol in milk matrices by high-performance liquid chromatography, *Journal of Pharmaceutical Analysis* **7** (2017) 401-405. https://doi.org/10.1016/j.jpha.2017.07.005

[6] H. N. K. Al-Salman, E. Q. Jasim, H. H. Hussein, F. H. Shari, Theophylline determination in pharmaceuticals using a novel high-performance liquid chromatographic process, *NeuroQuantology* **19** (2021) 196-208. https://doi.org/10.14704/nq.2021.19.7.NQ21103

[7] M. H. Ahmed, E. F. Elkady, S. T. Mahmoud, E. H. Mohamed, A green validated HPLC-UV Method for determining and quantifying pholcodine, paracetamol, and pseudoephedrine in laboratory-prepared mixtures and their FDC capsule, *Green Analytical Chemistry* **12** (2025) 100187. https://doi.org/10.1016/j.greeac.2024.100187

[8] M. Hosseini, R. Castillo, M. Soleymani, A novel magnetic-assisted ionic liquid-based microextraction method (MA-ILBME): Specific design system for sensitive spectrophotometric analysis of paracetamol as a pharmaceutical pollutant in environmental samples, *Talanta* **286** (2025) 127486. https://doi.org/10.1016/j.talanta.2024.127486
[9] E. Mari, M. Duraisamy, M. Eswaran, S. Sellappan, K. Won, P. Chandra, P.-C. Tsai, P.-C. Huang, Y.-H. Chen, Y.-C. Lin, V.K. Ponnusamy, Highly electrochemically active Ti_3C^2Tx MXene/ /MWCNT nanocomposite for the simultaneous sensing of paracetamol, theophylline, and caffeine in human blood samples, *Microchimica Acta* **191** (2024) 212. https://doi.org/10.1007/s00604-024-06273-9
[10] R. R. F. Fonseca, R. de Q. Ferreira, P. P. Luz, MOF-modified electrodes applied as electrochemical sensors for voltammetric determinations, *Journal of Solid State Electrochemistry* **29** (2025) 837-854. https://doi.org/10.1007/s10008-024-05985-5
[11] Zohaa, D. Arif, M. Hassan, M. Abdullah, W. Miran, M.A. Nasir, S. Batool, M.A. Baig, U. Liaqat, An electrochemical sensor based on copper oxide nanoparticles loaded on a mesoporous MCM-41 for non-enzymatic detection of glucose, *Ceramics International* **50** (2024) 12614-12620. https://doi.org/10.1016/j.ceramint.2024.01.171
[12] E. Zarei, M. Hadadi, A. Asghari, Z. Bahrami, Voltammetric Sensor for Simultaneous Determination of 4-Aminophenol, Acetaminophen and Mefenamic Acid Based on $CoFe_2O_4$/MCM-41 Nanocomposite Modified Electrode, *Surface Engineering and Applied Electrochemistry* **60** (2024) 857-873. https://doi.org/10.3103/S1068375524700479
[13] Ş. Kaya, V. Şimşek, S. Şahin, Investigation of Graphene Oxide/Mesoporous Silica Supports for Enhanced Electrochemical Stability of Enzymatic Electrodes, *Catalysis Letters* **154** (2024) 2701-2712. https://doi.org/10.1007/s10562-023-04520-x
[14] T. B. Benzaquén, P. M. Carraro, G. A. Eimer, J. Urzúa-Ahumada, P. S. Poon, J. Matos, Rice Husks as a Biogenic Template for the Synthesis of Fe_2O_3/MCM-41 Nanomaterials for Polluted Water Remediation, *Molecules* **30** (2025) 2484. https://doi.org/10.3390/molecules30122484
[15] Z. Zhang, W. Dong, Y. Huang, Oxidative degradation of chitosan by Fe-MCM-41 heterogeneous Fenton-like system, *Scientific Reports* **14** (2024) 25972. https://doi.org/10.1038/s41598-024-76520-9
[16] Y. Guo, B. Chen, Y. Zhao, T. Yang, Fabrication of the magnetic mesoporous silica Fe-MCM-41-A as efficient adsorbent: perfomance, kinetics and mechanism, *Scientific Reports* **11** (2021) 2612. https://doi.org/10.1038/s41598-021-81928-8
[17] M. Hasanzadeh, N. Shadjou, E. Omidinia, Mesoporous silica (MCM-41)-Fe_2O_3 as a novel magnetic nanosensor for determination of trace amounts of amino acids, *Colloids and Surfaces B: Biointerfaces* **108** (2013) 52-59. https://doi.org/10.1016/j.colsurfb.2013.02.015
[18] J. S. Beck, J. C. Vartuli, W. J. Roth, M. E. Leonowiz, C. T. Kresge, K. D. Schmitt, C. T. W. Chu, D. H. Olson, E. W. Sheppard, S. B. McCullen, J. B. Higgins, J. L. Schlenker, A new family of mesoporous molecular sieves prepared with liquid crystal templates, *Journal of the American Chemical Society* **114** (1992) 10834-10843. https://doi.org/10.1021/ja00053a020
[19] H. Naeimi, V. Nejadshafiee, M.R. Islami, Iron (III)-doped, ionic liquid matrix-immobilized, mesoporous silica nanoparticles: Application as recyclable catalyst for synthesis of pyrimidines in water, *Microporous and Mesoporous Materials* **227** (2016) 23-30. https://doi.org/10.1016/j.micromeso.2016.02.036
[20] M. Selvaraj, P. K. Sinha, K. Lee, I. Ahn, A. Pandurangan, T. G. Lee, Synthesis and characterization of Mn-MCM-41 and Zr-Mn-MCM-41, *Microporous and Mesoporous Materials* **78** (2005) 139-149. https://doi.org/10.1016/j.micromeso.2004.10.004
[21] H. Kosslick, G. Lischke, G. Walther, W. Storek, A. Martin, R. Fricke, Physico-chemical and catalytic properties of Al-, Ga- and Fe-substituted mesoporous materials related to MCM-41, *Microporous Materials* **9** (1997) 13-33. https://doi.org/10.1016/S0927-6513(96)00087-9

[22] M. Amal Raj, S. Abraham John, Graphene layer modified glassy carbon electrode for the determination of norepinephrine and theophylline in pharmaceutical formulations, *Analytical Methods* **6** (2014) 2181-2188. https://doi.org/10.1039/C3AY42279H
[23] A. S. Farag, Voltammetric determination of acetaminophen in pharmaceutical preparations and human urine using glassy carbon paste electrode modified with reduced graphene oxide, *Analytical Sciences* **38** (2022) 1213-1220. https://doi.org/10.1007/s44211-022-00150-2
[24] T. R. Saciloto, P. Cervini, É. T. G. Cavalheiro. Simultaneous voltammetric determination of acetaminophen and caffeine at a graphite and polyurethane screen-printed composite electrode, *Journal of the Brazilian Chemical Society* **24** (2013) 1461-1468. https://doi.org/10.5935/0103-5053.20130186
[25] D. M. Fernandes, N. Silva, C. Pereira, C. Moura, J. M. C. S. Magalhães, B. Bachiller-Baeza, I. Rodríguez-Ramos, A. Guerrero-Ruiz, C. Delerue-Matos, C. Freire. $MnFe_2O_4$@CNT-N as novel electrochemical nanosensor for determination of caffeine, acetaminophen and ascorbic acid. *Sensors and Actuators B: Chemical* **218** (2015) 128-136. https://doi.org/10.1016/j.snb.2015.05.003
[26] A. Arenas-Hernandez, F.E. Cancino-Gordillo, U. Pal, $Ni_{1-x}Mn_xCo_2O_4$ Nanoparticles as High-Performance Electrochemical Sensor Materials for Acetaminophen Monitoring, *ACS Omega* **10** (2025) 11250-11263. https://doi.org/10.1021/acsomega.4c10927
[27] B. Healy, F. Rizzuto, M. de Rose, T. Yu, C.B. Breslin, Electrochemical determination of acetaminophen at a carbon electrode modified in the presence of β-cyclodextrin: role of the activated glassy carbon and the electropolymerised β-cyclodextrin, *Journal of Solid State Electrochemistry* **25** (2021) 2599-2609. https://doi.org/10.1007/s10008-021-05044-3
[28] S. Perveen, J. A. Baig, M. Nur-e-Alam, M. Kazi, S. Memon, T. G. Kazi, K. Akhtar, S. Hussain, Electrocatalytic detection of Acetaminophen by sodium ferrite, *Results in Physics* **68** (2025) 108073. https://doi.org/10.1016/j.rinp.2024.108073
[29] L. Zhang, T. Wang, X. Fan, D. Deng, Y. Li, X. Yan, L. Luo, Simultaneous Determination of Theophylline and Caffeine Using Poly(L-phenylalanine)-Reduced Graphene Oxide Modified Glassy Carbon Electrode, *International Journal of Electrochemical Science* **16** (2021) 21041. https://doi.org/10.20964/2021.04.22
[30] S. Sabilla, P.K. Jiwanti, T. Kondo, R. Akiyama, T. Kusunoki, A. A. Afkauni, A. S. Latifah, Arramel, T. Amrillah, Y. W. Hartati, Q. K. Anjani, Y. M. T. A. Putri, J. Gunlazuardi, Sensitive and Selective Theophylline Electrochemical Detection on ZnO Nanoflowers/Graphene Oxide/Boron-Doped Diamond Nanoparticles, *ACS Omega* **10** (2025) 27435-27447. https://doi.org/10.1021/acsomega.5c03180
[31] A. Dhamodharan, K. Perumal, Y. Gao, H. Pang, Sensitive Detection of Theophylline Using a Modified Glassy Carbon Electrode with g-C_3N_4, *Chemistry Africa* **7** (2024) 5087-5096. https://doi.org/10.1007/s42250-024-01094-y
[32] E. Sharifi Pour, M. Ebrahimi, H. Beitollai, Electrochemical Sensing of Theophylline using Modified Glassy Carbon Electrode, *Chemical Methodologies* **6** (2022) 560-568. https://doi.org/10.22034/chemm.2022.336988.1476
[33] P. Di Matteo, A. Trani, M. Bortolami, M. Feroci, R. Petrucci, A. Curulli, Electrochemical Sensing Platform Based on Carbon Dots for the Simultaneous Determination of Theophylline and Caffeine in Tea, *Sensors* **23** (2023). https://doi.org/10.3390/s23187731